Parallel fractional correlation: an optical implementation

Sergio Granieri, Myrian Tebaldi, and Walter D. Furlan

An optical setup to obtain all the fractional correlations of a one-dimensional input in a single display is implemented. The system works as a multichannel parallel correlator for a continuous set of fractional orders and presents a variable shift variance. Some experimental results together with computer simulations are performed to illustrate the performance of our proposal. © 2001 Optical Society of America

OCIS codes: 070.0070, 100.5010, 070.2590.

1. Introduction

Among several mathematical operations that can be optically implemented, correlation is one of the most important because it can be used for different applications, such as pattern recognition and object localization. Optical correlation can be performed by use of the Fourier transform property of coherent optical systems. To implement this operation, several optical architectures were developed, such as the classical VanderLugt and joint transform correlators.[1,2] Because conventional correlation is a shift-invariant operation, the correlation output simply moves if the object translates at the input plane. In many cases this property is necessary, but there are situations in which the position of the object provides additional information (for example, in image coding or cryptographic applications), and so shift invariance is a disadvantage.

The fractional correlation is a generalization of the classical correlation that employs, instead of the conventional Fourier transform, the optical fractional Fourier transform (FRT) of a given fractional order p.[3,4] This operation was optically implemented by Mendlovic *et al.*[5,6] and was generalized in Refs. 7 and 8. In these studies the fractional correlation is obtained as the inverse Fourier transform of the product of both the FRTs of the reference and input objects, but for a single fractional order p at a time. The fractional order involved in the FRT controls the amount of shift variance of the correlation. As is well known, the shift-variance property modifies the intensity of the correlation output when the input is shifted. In several pattern-recognition applications this feature is useful, for example, when an object should be recognized in a relevant area and rejected otherwise or when the recognition should be based on certain pixels in systems with variable spatial resolution. However, the optimum amount of variance for a specific application is frequently difficult to predict, and therefore more complete information would certainly be attained from a display showing several fractional correlations at the same time. Ideally, such a display should include the classical shift-invariant correlation as the limiting case. That is the motivation of this paper; here we extend the ideas proposed in Ref. 8 to present an optical multichannel fractional correlator. The proposed optical system generates a simultaneous display of fractional correlations of a one-dimensional (1-D) input for a continuous set of fractional orders in the range [0, 1]. In Section 2 we first describe the optical arrangement used to record continuous multichannel fractional filters, and then we show how the same setup can be modified to implement a parallel fractional correlator. In Section 3 we show experimental results and numerical simulations obtained with the described proposal.

S. Granieri and M. Tebaldi are with the Centro de Investigaciones Ópticas, P.O. Box 124, (1900) La Plata, Argentina. W. D. Furlan (e-mail address: walter.furlan@uv.es) is with the Departamento de Óptica, Universitat de València, E-46100 Burjassot, Spain.

Received 1 August 2000; revised manuscript received 4 December 2000.

0003-6935/01/356439-06$15.00/0

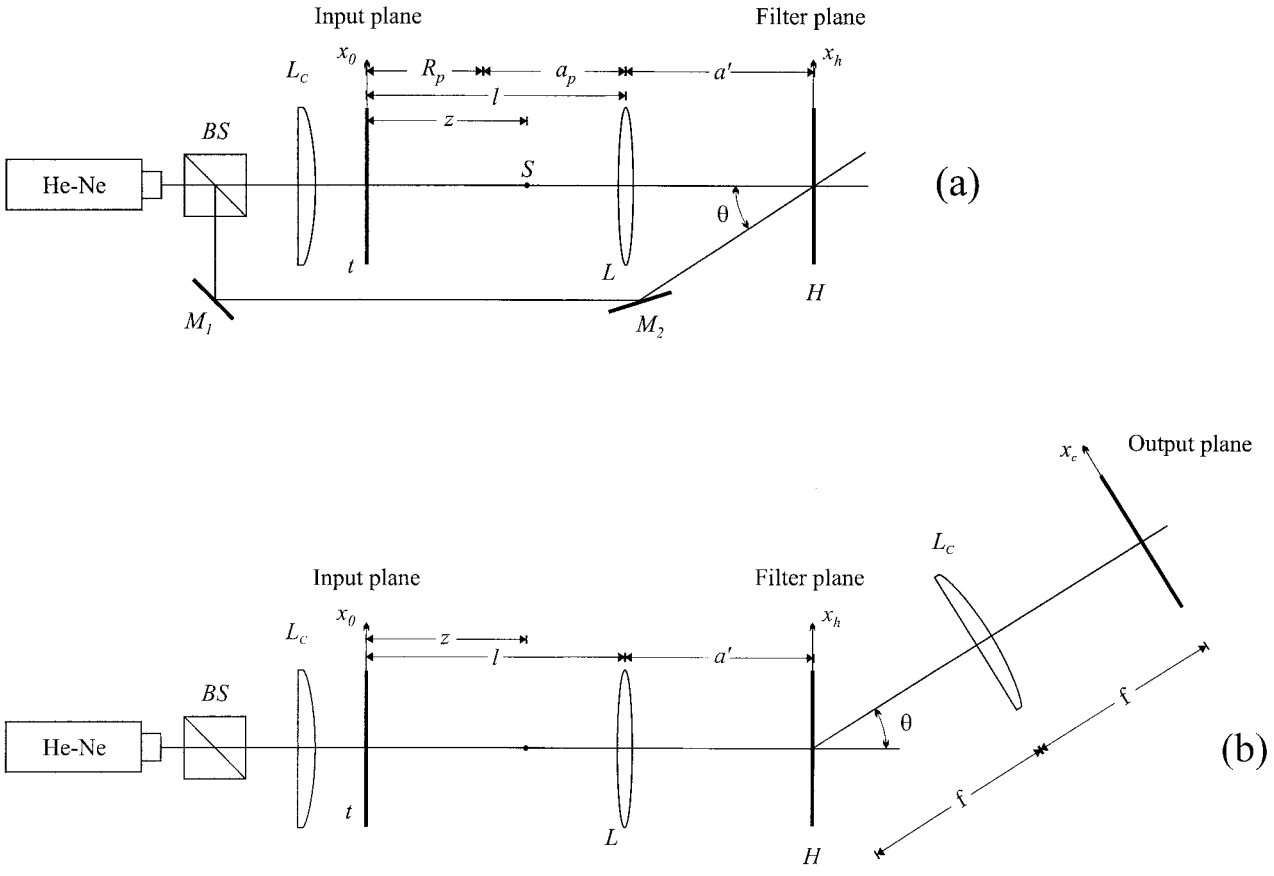

Fig. 1. Top view of the optical setups to achieve (a) the filter H, which stores the Radon–Wigner display of the 1-D input $t(x_0)$ and (b) the parallel fractional correlation between $t(x_0)$ and $t(x_0 + \Delta)$ at the output plane. M_1 and M_2, mirrors; BS, beam splitter; L, varifocal lens; L_C, cylindrical lens.

2. Parallel Fractional Correlation

The FRT of order p of a given two-dimensional (2-D) function $f(x_0, y_0)$, defined mathematically as

$$\mathcal{F}^p\{f(x, y)\} = \frac{i \exp(ip\pi/2)}{\sin(p\pi/2)} \exp\left[\frac{i\pi(x^2 + y^2)}{\tan(p\pi/2)}\right] \times \int\int_{-\infty}^{\infty} f(x_0, y_0) \exp\left[\frac{i\pi({x_0}^2 + {y_0}^2)}{\tan(p\pi/2)}\right] \times \exp\left[-\frac{i2\pi(xx_0 + yy_0)}{\sin(p\pi/2)}\right] \mathrm{d}x_0 \mathrm{d}y_0, \tag{1}$$

can be optically obtained by free-space propagation of an spherical wave front impinging on a input transparency with amplitude transmittance $t(x_0, y_0) = f(x_0/s, y_0/s)$, where s is the scale parameter used for the construction of the transparency. In effect, as was stated in Refs. 9 and 10 and demonstrated experimentally in Ref. 11, every Fresnel diffraction pattern of the transparency illuminated with a monochromatic point source corresponds to a scaled version of a certain FRT of the same input and vice versa. The mathematical relationship between the Fresnel diffraction field, obtained at distance R_p of the input illuminated with a spherical wave front of radius z and wavelength λ, and the FRT of order p, of the input function, is given by[10,12]

$$U_{z_p, R_p}(x, y) = \exp\left\{\frac{-i\pi(x^2 + y^2)}{\lambda}\left[\frac{z(1 - M_p) - R_p}{z\,{M_p}^2\,R_p}\right]\right\} \times \mathcal{F}^p\left\{t\left(\frac{x_0}{M_p}, \frac{y_0}{M_p}\right)\right\}, \tag{2}$$

where M_p is the magnification of the optical FRT. For each fractional order the values of M_p and R_p are related to the system parameters, s, λ, and z through

$$R_p = \frac{s^2\lambda^{-1} \tan p\pi/2}{1 + s^2(\lambda z)^{-1} \tan p\pi/2}, \tag{3}$$

$$M_p = \frac{1 + \tan p\pi/2 \tan p\pi/4}{1 + s^2(\lambda z)^{-1} \tan p\pi/2}. \tag{4}$$

Equations (2)–(4) allow one to recognize that by illumination of an input transparency with a spherical wave front converging to an axial point S, all the FRT in the range [0, 1] can be obtained simultaneously, apart from a quadratic phase factor and a scale factor. The FRTs are axially distributed between the input transparency ($p = 0$) and the virtual source S ($p = 1$) in which the optical Fourier transform of the input is obtained.

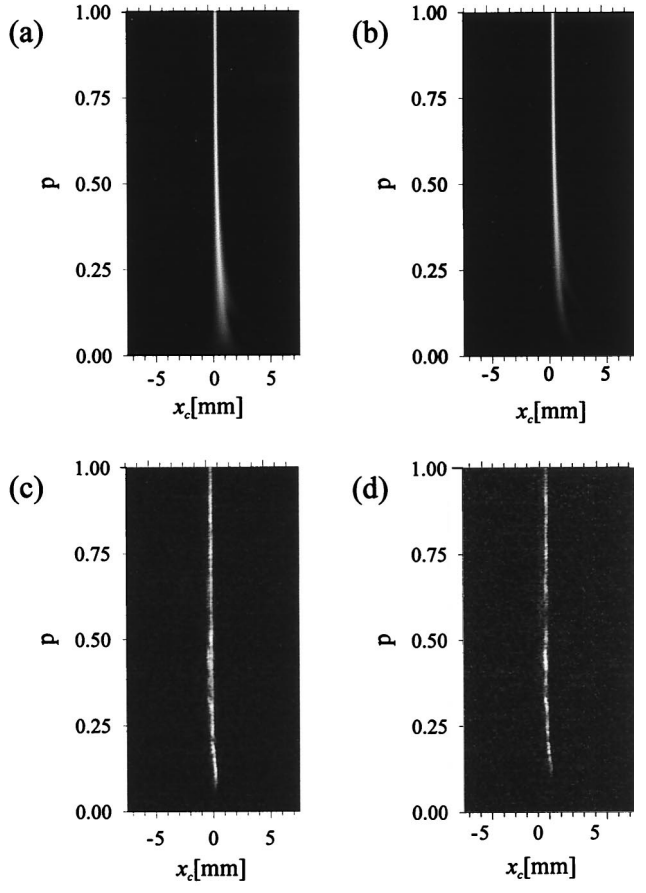

Fig. 2. Intensity patterns of the output plane of the correlator: (a) and (b) computer simulations for displacements $\Delta = 0.5$ mm and $\Delta = 0.7$ mm, respectively; (c) and (d) experimental results.

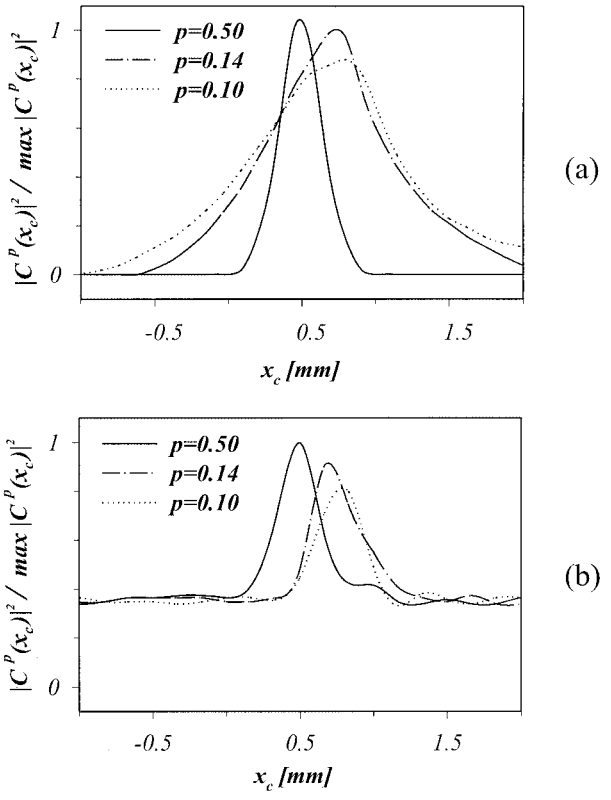

Fig. 3. Normalized fractional correlations for several fractional orders p obtained from different slices of the intensity distributions shown in Figs. 2(a) and 2(c) for the case of $\Delta = 0.5$ mm: (a) numerical results; (b) experimental results.

As was shown in Ref. 13, for 1-D signals the optical FRTs can be displayed simultaneously in a single 2-D chart in which one axis is the fractional order p and the other axis x is the coordinate transversal to the direction of propagation. This kind of representation, called the Radon–Wigner display, provides the basis for multichannel operations on 1-D signals. The optical setup to obtain it is represented in Fig. 1(a). A 1-D input, $t(x_0)$, is illuminated by a cylindrical wave front (generated by the lens L_C) converging to a line segment normal to the optical axis S. According to Eq. (3), the FRTs of orders ranging in the interval [0,1] are located at distances R_p from the input with a scale factor given by Eq. (4). In this way each plane between the input and S contains a different scaled 1-D FRT of the object. The optical element L is a lens designed to image the axially distributed FRT channels at one time in a single plane. Consequently, its focal distance must be different for each value of the y coordinate, normal to the plane in Fig. 1. Although the magnification for every fractional order at the output plane could never be simultaneously the proper one, a quite good approximation can be obtained with a commercially available ophthalmic lens. The limits of this approximation have been already discussed in Ref. 13 in which it was shown that the power of this lens is fixed by the constraint conditions that the distances z, l, and a' in Fig. 1 must satisfy [see Eqs. (16) and (17) of Ref. 13. Then with the assumption that the object distance for each 1-D channel (order p) is a_p and that the image distance for the same channel is a', the exact relationship between the FRT and the Fresnel diffraction pattern at the filter plane in Fig. 1(a) is the following,

$$U_h(x) = \exp\left\{-i\pi \frac{x_h^2}{\lambda}\left[\frac{z\,(1 - M_p^2) - R_p}{z\,R_p} + \frac{1}{a'} + \frac{1}{a_p M_L^2}\right]\right\} \mathcal{F}^p\{t(x_0)\}, \tag{5}$$

where M_L is the magnification introduced by the varifocal lens L,

$$M_L(p) = \frac{a'[1 - s^2(\lambda z)^{-1} \tan p\pi/2]}{l\left[1 - s^2(\lambda)^{-1} \tan p\pi/2\left(\frac{1}{z} - \frac{1}{l}\right)\right]}, \tag{6}$$

which compensates for the scale error given in Eq. (2): i.e., $M_p M_L \simeq -1$.

By use of the spectral domain, the fractional cor-

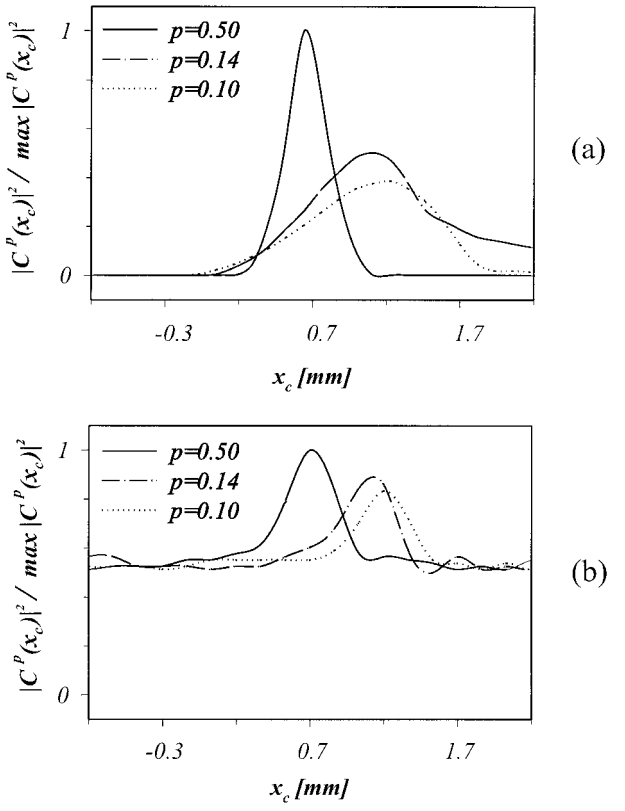

Fig. 4. Normalized fractional correlations for several fractional orders p obtained from different slices of the intensity distributions shown in Figs. 2(b) and 2(d) for the case of $\Delta = 0.7$ mm: (a) numerical results; (b) experimental results.

relation between two 1-D functions $t(x)$ and $t'(x)$ is defined as[5]

$$C^p(x) = \mathcal{F}^{-1}\{\mathcal{F}^p\{t(x_0)\}\ \mathcal{F}^{p*}\ \{t'(x_0)\}\}, \qquad (7)$$

where $\mathcal{F}^p\ \{\ \}$ represents the FRT operator defined by Eq. (1) and $\mathcal{F}^{p*}\ \{\ \}$ is its complex conjugate. It is easy to show that all the phase terms involved in the FRT definition cancel out in Eq. (7). Moreover, with the above definition the classical correlation is obtained if we set $p = 1$.

The product inside the outer brackets of Eq. (7) can be optically achieved simultaneously for all fractional orders, ranging between $p = 0$ and $p = 1$, following a two-step process. In the first stage, with the experimental configuration shown in Fig. 1(a), all the FRTs of $t(x_0)$ are obtained in parallel at the filter plane by means of the varifocal lens L by a proper selection of the parameters z, l, a' in Eq. (4). A matched filter is obtained at this plane by recording an hologram of these FRTs with a reference wave front at an angle θ. In the second stage, the obtained multichannel-matched filter is located at the filter plane, and the input function to be correlated is located at the input plane [see Fig. 1(b)]. Because the transmittance of the holographic filter has one term proportional to the complex conjugate of the field in Eq. (5), for each fractional order channel, the field immediately behind the filter plane has one term proportional to the product of the complex conjugate of the FRT of the reference function $t'(x_0)$ and the FRT of the input function $t(x_0)$. Thus the multiplicative phase factor in Eq. (5) and the corresponding one of the matched filter cancel out. Besides, although the experimental FRT for a given order p is approximated owing to the scale error, the experimental fractional correlation can be obtained exactly because this error affects both $\mathcal{F}^p$ and $\mathcal{F}^{p*}$. This property can be proved simply by incorporating Eq. (5) into Eq. (7). Finally, the diffracted field at the angle θ is collected by the lens L_C, which performs a 1-D Fourier transform. Because each fractional order p, ranging between $p = 0$ and $p = 1$, has an independent 1-D correlation channel, all the fractional correlations for this range of p are obtained simultaneously at the output plane [see Eq. (7)]. Thus a 2-D display is obtained in which the fractional correlations are ordered in a continuous display along the axis normal to the plane shown in Fig. 1(b). It must be emphasized that the fractional correlation obtained by the optical arrangement of Fig. 1 is free from the scale and phase errors introduced by the optical generation of the FRT, but only when the fractional orders are equal. The exact cross-fractional correlation[8] cannot be implemented with this proposal because the phase terms will not cancel out.

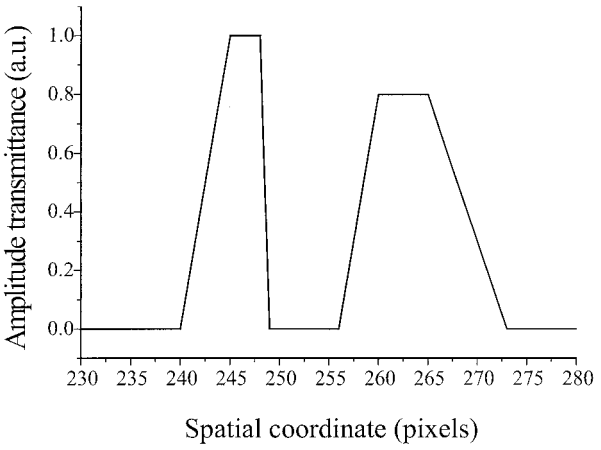

Fig. 5. Amplitude transmittance of the nonsymmetric double slit.

3. Experimental Results and Discussion

To illustrate the use of the parallel fractional correlator, we perform a simple experiment to analyze the shift-variant property of the FRT. To accomplish this, we obtain the optical fractional correlations between a rectangle function (the reference),

$$t(x_0) = \mathrm{rect}(x_0/a),$$

with $a = 1$ mm, and a shifted version of it (the input),

$$t'(x_0) = t(x_0 + \Delta),$$

using the experimental setup shown in Fig. 1. In the first step an holographic filter H [see Fig. 1(a)] stores the Radon–Wigner display associated with the

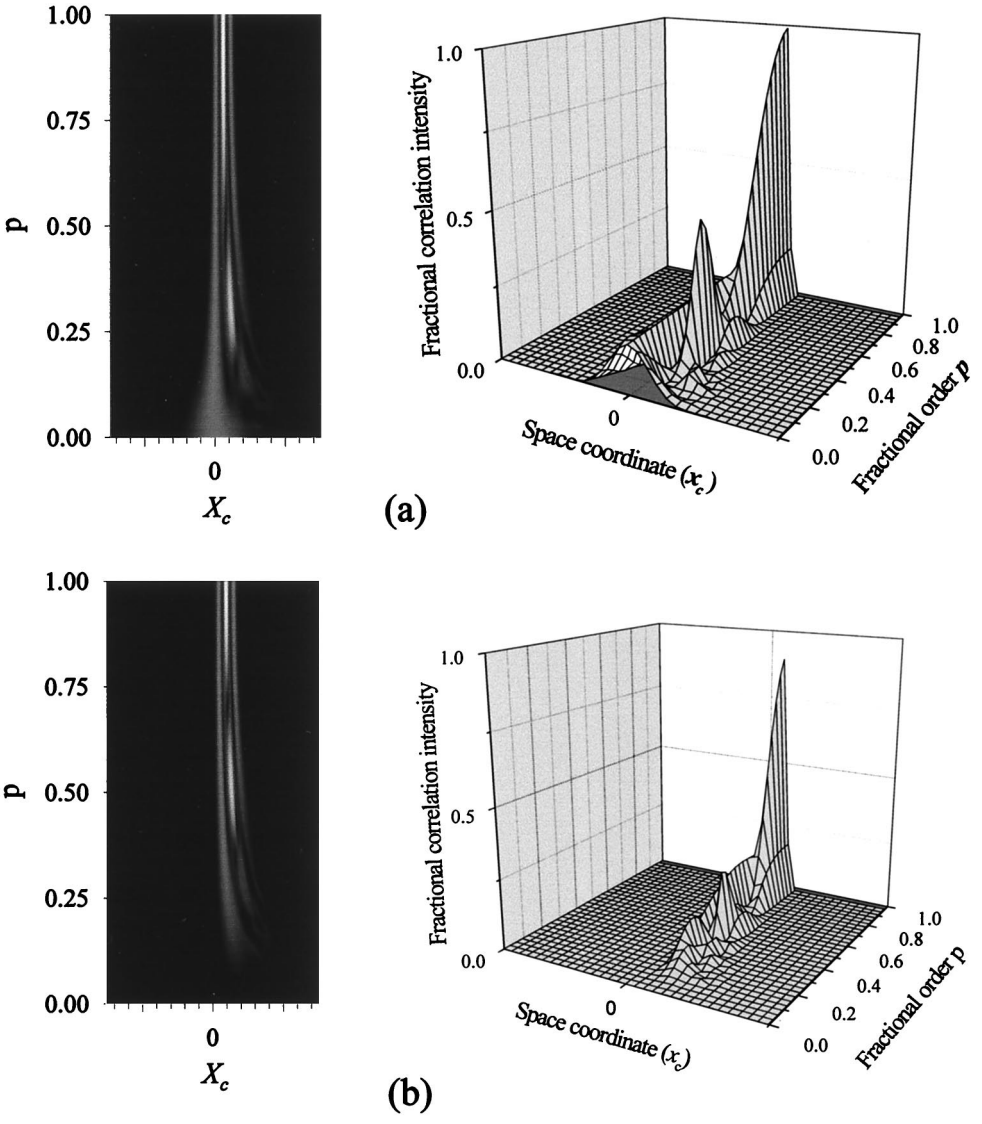

Fig. 6. Fractional correlations for several fractional orders p obtained at the output plane of the setup of Fig. 1. Intensity patterns as a gray level (left), and the corresponding three-dimensional plot (right). The filter is registered for the double slit of Fig. 5. The input is the same object but with two different shifts (see the main text).

2-D version of $t(x_0)$. An expanded and collimated He–Ne laser beam is used as a light source from which the beam splitter (BS) produces two coherent beams. One of them generates the Radon–Wigner transform of the input at the filter plane[13] while the other is used as reference light beam at the angle θ. The object transparency is illuminated through a cylindrical lens focusing at the axial point S, and the varifocal lens L is an ophthalmic progressive lens of power +2.75D and +5.75D in the so-called distance portion and near portion, respectively. The relevant distances in the optical system are $z = 426$ mm, $l = 646$ mm, and $a' = 831$ mm. In the second step the optical system is slightly modified as is shown in Fig. 1(b); a lens L_C, in a 2-f configuration along the x coordinate, is added to obtain the multiple correlation at the output plane. In the experiments the input transparency is translated a fixed length, Δ, along the x_0 axis to simulate a transversal shift. A CCD camera is used to acquire the experimental data at the output plane. Two different positions of the input object were investigated: $\Delta = 0.5$ mm, and $\Delta = 0.7$ mm. Figure 2 shows the respective intensity patterns at the correlation plane computed numerically, Figs. 2(a) and 2(b), and the corresponding experimental results, Figs. 2(c) and 2(d). A profile along a line parallel to the x_c axis, in the displays of Fig. 2, corresponds to the fractional correlation of a single order p. As can be seen, for a fixed displacement Δ, the correlation peak decreases for p decreasing. As expected for $p = 1$, the correlation peak is the classical one located at the input position. For values ranging between $p = 1$ and $p = 0.5$, the correlation peak did not change appreciably. Even for the small shifts in our experiment, the shift-variant property becomes evident for values $p \leq 0.25$. In Figs. 3 and

4 we show the profile peaks of the fractional correlation, for several fractional orders p, obtained from Fig. 2. It can be seen that as p becomes lower the peak degenerates and shifts disproportionately toward the object position.

In a second example a more complex object is used as a reference object. The amplitude transmittance of this object is shown in Fig. 5. It represents a double (nonsymmetric) slit with a continuous gray-level amplitude transmittance. The continuous transition between the shift-variant case ($p = 0$) to the shift-invariant case ($p = 1$) is confirmed in Fig. 6 in which the numerical simulation of the fractional correlation, when the reference object is shifted a fixed amount at the input plane, is considered. Figure 6(a) shows the fractional correlations when the input is shifted an amount of one-half of the object size, and Fig. 6(b) shows the fractional correlation when the input is shifted an amount equal to the size of the object. The variant behavior of the fractional correlation can be clearly seen when Fig. 6(a) is compared with Fig. 6(b). Both displays coincide near to $p = 1$ (except for the location of the maxima), but for lower values of p the fractional correlation is highly dependent on the magnitude of the shift.

Summarizing, we have proposed and experimentally implemented an optical setup for obtaining the fractional correlations for a continuous set of fractional orders. The output of the system shows a variable degree of space variance ranging from the pure shift-variance case ($p = 0$) to the pure shift-invariance case ($p = 1$, classical correlation). This kind of representation provides information about the object, such as classical correlation, but also quantifies its departure from a given reference position.

Financial support from Conselleria de Cultura Educaciò i Ciència, Generalitat Valenciana, Spain, project GV99-100-1-01, and from Agencia Nacional de Promoción Científica y Tecnológica, Secretaría de Ciencia y Tecnología, Argentina, project PMT-PICT 0289, is gratefully acknowledged. S. Granieri and M. Tebaldi thank the research fellowship program of the Universidad Nacional de La Plata, Argentina. The ophthalmic varifocal lens used in the experiments was kindly provided by INDO S.A.

References

1. A. Vander Lugt, *Optical Signal Processing* (Wiley, New York, 1992).
2. J. W. Goodman, *Introduction to Fourier Optics* (McGraw Hill, New York, 1996).
3. W. Lohmann, "Image rotation, Wigner rotation, and the fractional Fourier transform," J. Opt. Soc. Am. A **10,** 2181–2186 (1993).
4. D. Mendlovic and H. M. Ozaktas, "Fractional Fourier transformations and their optical implementation. I," J. Opt. Soc. Am. A **10,** 1875–1881 (1993).
5. D. Mendlovic, H. M. Ozaktas, and A. W. Lohmann, "Fractional correlation," Appl. Opt. **34,** 303–309 (1995).
6. D. Mendlovic, Y. Bitran, R. G. Dorsch, and A. W. Lohmann, "Optical fractional correlation: experimental results," J. Opt. Soc. Am. A **12,** 1665–1670 (1995).
7. A. W. Lohmann, Z. Zalevsky, and D. Mendlovic, "Synthesis of pattern recognition filters for fractional Fourier processing," Opt. Commun. **128,** 199–204 (1996).
8. S. Granieri, R. Arizaga, and E. E. Sicre, "Optical correlation based on the fractional Fourier transform," Appl. Opt. **36,** 6636–6645 (1997).
9. P. Pellat-Finet, "Fresnel diffraction and the fractional-order Fourier transform," Opt. Lett. **19,** 1388–1390 (1994).
10. P. Andrés, W. D. Furlan, G. Saavedra, and A. W. Lohmann, "Variable fractional Fourier processor: a simple implementation," J. Opt. Soc. Am. A **14,** 853–858 (1997).
11. J. Hua, L. Liu, and G. Li D, "Observing the fractional Fourier transform by free-space Fresnel diffraction," Appl. Opt. **36,** 512–513 (1997).
12. E. Tajahuerce, G. Saavedra, W. D. Furlan, E. Sicre, and P. Andrés, "White-light optical implementation of the fractional Fourier transform with adjustable order control," Appl. Opt. **39,** 238–247 (2000).
13. S. Granieri, W. D. Furlan, G. Saavedra, and P. Andrés, "Radon–Wigner display: a compact optical implementation with a single varifocal lens," Appl. Opt. **36,** 8363–8369 (1997).